Hindawi
Advances in Materials Science and Engineering
Volume 2018, Article ID 2352864, 11 pages
https://doi.org/10.1155/2018/2352864

Research Article

Mesoscopic Finite Element Method of the Effective Thermal Conductivity of Concrete with Arbitrary Gradation

Pingming Huang,[1] Yu Zhao,[1] Yanwei Niu,[1] Xiang Ren,[2] Mingfeng Chang,[3] and Yamin Sun[1]

[1]*School of Highway, Changan University, Xian 710064, China*
[2]*School of Architecture and Civil Engineering, Xian University of Science and Technology, Xian 710064, China*
[3]*School of Materials Science and Engineering, Changan University, Xian 710064, China*

Correspondence should be addressed to Yamin Sun; sunyamin@chd.edu.cn

Received 4 June 2018; Revised 20 November 2018; Accepted 5 December 2018; Published 27 December 2018

Academic Editor: Paolo Andrea Carraro

The effective thermal conductivity (ETC) of concrete is the most important parameter in determining the temperature field and thermal stresses. A 2D random polygonal aggregate model and its modified model considering porosity were established in this paper in order to partially replace the experiment for parametric analysis on the ETC of concrete and to save the experiment cost. A mesoscopic finite element method for the ETC of concrete with arbitrary gradation was also proposed. In addition, the influence factors (thermal conductivity of coarse aggregate, cement mortar, and volume fraction of coarse aggregate) of the effective thermal conductivity of concrete were analyzed. The results show that the 2D gradation curve of coarse aggregates is proved to exist, and there is a corresponding relationship between the 2D and 3D gradation curves of coarse aggregates. The effective thermal conductivity of concrete has a positive exponential relationship with the volume fraction of coarse aggregates, a positive logarithm relationship with the thermal conductivity of coarse aggregates, and a positive linear correlation with the thermal conductivity of cement mortar. The most practical way to improve the effective thermal conductivity of concrete is to increase the ETC of the cement mortar, but the most effective way is to replace the aggregate with a material with a high thermal conductivity.

1. Introduction

Estimating the heat transfer properties of concrete is of great significance in various engineering fields, such as building energy conservation [1, 2], hydraulic structures, nuclear reactor structures [3], bridge structures, and other structures exposed under the thermal loading [4]. The effective thermal conductivity of concrete is the most important parameter in denoting the thermal transmission capacity of concrete and in determining the temperature field in concrete structure. Large temperature gradient due to the low ETC of concrete would induce considerable thermal stresses, which will probably lead to cracking in concrete structures. Hence, estimating the ETC of concrete accurately is important to prevent cracking and ensure the safety of concrete structures.

Previous studies on the ETC of concrete can be divided into three categories: experimental investigation, theoretical model, and mesoscopic finite element model. The experimental investigation indicated that moisture content, water-cement ratio (W/C), age, volume fractions of fine and coarse aggregates, and temperature had significant influence on the ETC of concrete [5–7]. Khan [8] measured the thermal conductivity of concrete at various moisture contents, and developed a relationship between the ETC of concrete and the thermal conductivity of aggregate at different saturations. Kim et al. [9] and Zhang et al. [10] investigated quantitatively the influence factors on the ETC of concrete and proposed different prediction equations for the ETC of concrete. Experimental investigation on the ETC of concrete is the most direct and effective method, but it can be time-consuming, costly, and labor intensive for investigating

plentiful concrete specimens. Concrete was regarded as a two-phase composite material consisting of cement mortar (continuous phase) and coarse aggregate (dispersed phase) in the mesoscale [8], and several theoretical models for the ETC of concrete were developed based on the two-phase composite material theory. Campbell-Allen and Thorne [11] considered concrete as a set of cubes of aggregate with uniform size arranged systematically in the matrix of cement mortar, and developed a simplified theory model (namely, Campbell-Thorne model) to calculate the ETC of concrete. Another theoretical model for the ETC of concrete was established on the basis of general model of porous materials, and the representative model was Harmathy model [12]. In addition, some semitheoretical models were developed based on the experimental results. The Hamilton–Crosser model included the effect of aggregate shapes [13]. The Bruggeman model considered the effect of aggregate volume fraction [14]. The Hasselaman-Johnson model took the effect of interfacial thermal resistance into account [15]. The ETC of concrete can be roughly estimated using these theoretical or semitheoretical models; however, they were derived based on many assumptions. Mesoscopic finite element method has been widely employed to study the mechanical behavior of concrete by simulating the anisotropic property of concrete. And the numerical results obtained from mesoscopic finite element method were in good agreement with the experimental results. And the numerical results obtained from the mesoscopic finite element method were in good agreement with the experimental results [16–19]. Thus, this mesoscopic finite element method was also used to simulate the thermal behavior of concrete [20, 21]. A two-dimensional numerical model was developed to calculate the ETC by Tang et al. [22], and the results revealed that the ETC of concrete depended on the degree of heterogeneity strongly, and the size and shape of coarse aggregates had negligible influence on the ETC of concrete. Carson et al. [23] established a two-dimensional mesoscopic finite element model to examine the influences of porosity on the ETC of theoretical porous materials, which simulated a steady-state thermal conductivity measurement device. Shen et al. [3] proposed a two-dimensional mesoscopic numerical method that evaluated the effect of cracking behavior on the ETC of concrete quantitatively. The results displayed that the effective thermal conductivity decreased greatly when some microcracks initiated, and the concrete became anisotropic as the microcracks propagated further. The mesoscopic finite element model can simulate the concrete material more accurately compared to the existing theoretical or semitheoretical models, and the numerical results match well with the experimental values. Theoretically, the mesoscopic finite element models can replace the experimental tests for parametric analysis on the ETC of concrete. However, the existing mesoscopic numerical model of concrete cannot consider the arbitrary gradation of coarse aggregates except for the fuller gradation [24], and the gradation of concrete has a significant effect on the degree of heterogeneity, which further affects the ETC of concrete. Besides, the mesoscopic finite element model has not been verified by experiments. Therefore, the mesoscopic numerical method in estimating the ETC of concrete still has great large application limitations.

This paper mainly consists of four steps. Firstly, a method generating two-dimensional random polygonal aggregate model of concrete with arbitrary gradation was proposed. Secondly, a mesoscopic numerical analysis method for the ETC of concrete was presented. Thirdly, the existing experiment results about the ETC of concrete were used to verify the validity of the proposed method. Finally, the influence of volume fraction and thermal conductivity of coarse aggregates and cement mortar on the ETC of concrete were investigated by the mesoscopic finite element method.

2. Mesoscopic Numerical Method

2.1. 2D Random Polygonal Aggregate Model for Concrete with Arbitrary Gradation. Generally, the aggregate volume fraction of bridge concrete is between 30% and 50%, and the artificial broken stones are used as coarse aggregates. A 2D random polygonal aggregate model can represent the section from an actual concrete structure accurately, as shown in Figure 1. However, the key of this model is to determine the 2D cumulative distribution function (CDF) of the coarse aggregates of concrete with arbitrary gradation. But the CDF of coarse aggregates is a 3D concept, and there is no 2D CDF concept currently. In this research, the 2D CDF is defined as the distribution of different aggregate sizes in the concrete section, which includes the cumulative distribution function of mass, area, and particle number (PNCDF). The 2D PNCDF of coarse aggregates can be determined as follows:

(i) A 3D random spherical aggregate model of concrete is generated according to the arbitrary gradation of coarse aggregates determined by the seiving test. The generation process was described by Ruan and Pan [25].

(ii) A random cross section is obtained from the 3D model.

(iii) A 2D PNCDF of coarse aggregates can be acquired by counting the particle number with different particle sizes in the cross section.

The development of a 2D random polygonal aggregate model of concrete is shown in the flow chart in Figure 2. Two parts are included in the flow chart: generating process and throwing process of coarse aggregate (determining the position of coarse aggregate) in the matrix of cement mortar. In the generating process of coarse aggregates, polygonal aggregate particles meeting the specified gradation conditions are generated according to the specified fraction of aggregate volume and the specified 2D size of model. At the same time, the polygonal aggregate parameters are stored in a predesigned matrix. In the throwing process of coarse aggregates, all the polygonal aggregate particles are put into the mortar matrix. In other words, the 2D random polygonal aggregate model of concrete is plotted according to the stored data. Only the 2D size S and the coarse aggregate volume fraction Ra need to be inputted. However, the minimum particle size in the 2D PNCDF is close to zero.

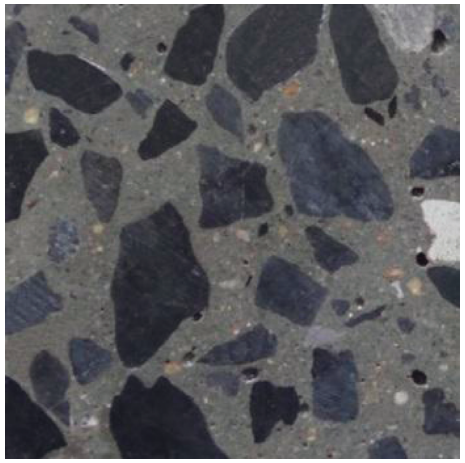

Figure 1: The section from an actual concrete.

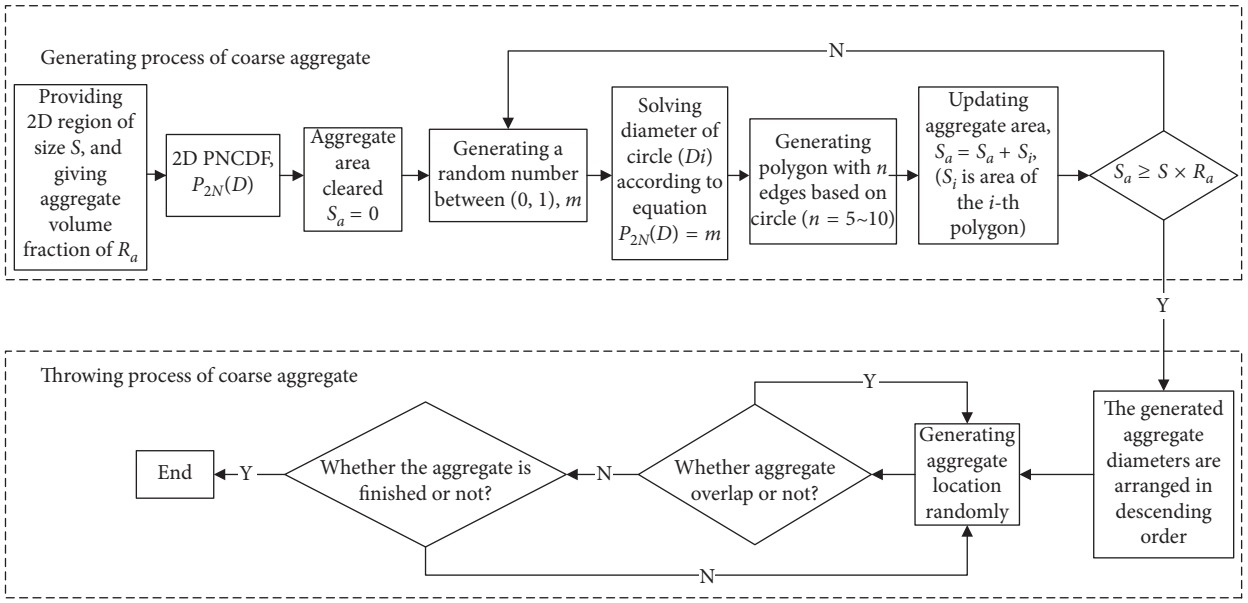

Figure 2: Generating process of the 2D random polygonal aggregate model.

Actually, the aggregates with a particle size less than 2 mm are regarded as fine aggregates. Therefore, the 2D PNCDF of coarse aggregates is modified by changing the particle size range to $(2, D_{\max})$.

L-RC2 specimen (the crushed limestone with particle sizes of 5–16 mm) was selected from Zhang's experiment [10], in order to illustrate the implementation of 2D random polygonal aggregate model. The 2D random polygonal aggregate model of a slice-cut was conducted by the method described above.

2.1.1. 3D Random Spherical Aggregate Model. The size distribution of coarse aggregates in a specimen is described by CDF $P_{3M}(D)$ with respect to the particle size D. Assuming a constant aggregate density ρ, then the CDF of particle volume $P_{3V}(D)$ is equal to $P_{3M}(D)$. For the L-RC2 specimen, $P_{3M}(D)$ and $P_{3V}(D)$ are given by

$$P_{3M}(D) = P_{3V}(D) = \frac{D^{\alpha} - D_{\min}^{\alpha}}{D_{\max}^{\alpha} - D_{\min}^{\alpha}}, \tag{1}$$

where α is a shape coefficient of the CDF. Equation (1) covers the Fuller curve for $\alpha = 0.5$ and $D_{\min} = 0$.

And the associated density function of particle volume $p_{3V}(D)$ is

$$p_{3V}(D) = \frac{dP_{3V}(D)}{dD} = \frac{\alpha D^{\alpha-1}}{D_{\max}^{\alpha} - D_{\min}^{\alpha}}. \tag{2}$$

In the different interval of $[D, D + dD]$, the increment of particle number $p_{3N}(D)$ is calculated by Equation (3):

$$p_{3N}(D) = \frac{p_{3V}(D)}{V(D)}, \tag{3}$$

where $V(D)$ is the volume of a spherical aggregate with diameter of D.

$$V(D) = \frac{1}{6}\pi D^3. \tag{4}$$

Then, the particle number CDF is defined as

$$P_{3N}(D) = \frac{\int_{D_{\min}}^{D} p_{3N}(D)}{\int_{D_{\min}}^{D_{\max}} p_{3N}(D)}, \tag{5}$$

substituting the parameter values of L-RC2 into equation (5), the result is described in equation (6)

$$P_{3N}(D) = \frac{D^{\alpha-3} - 5^{\alpha-3}}{16^{\alpha-3} - 5^{\alpha-3}}. \tag{6}$$

According to the generating process of the 3D random aggregate model by Ruan et al. [25], the 3D random spherical aggregate model of L-RC2 is developed and shown in Figure 3($\alpha = 0.5$).

2.1.2. 2D CDF of Particle Number. The cross section of a 3D random spherical aggregate model can provide the geometry of 2D circular model; then, a 2D PNCDF can also be obtained by counting the particle number of different particle size intervals in this cross section. In fact, only coarse aggregate parameters such as minimum and maximum particle size ($D_{\min}$ and $D_{\max}$) are the influence factors for the gradation curve. Therefore, it is assumed that the 2D aggregate gradation curve is only related to these parameters but independent of the size of 3D random spherical aggregate model, cross-sectional position from 3D model, and volume fraction of coarse aggregates.

To verify the validity of this assumption, the PNCDFs of five different cross sections along the height direction (1/6H, 2/6H, 3/6H, 4/6H, and 5/6H, where H is total thickness of the specimen.) were counted firstly, and six random aggregate models were established to eliminate the effect of randomness on the PNCFD. The average PNCFD from six models was taken as the PNCFD of the cross section, as shown in Figure 4. The results show that the PNCDFs of coarse aggregates are almost the same at 2/6H, 3/6H, and 4/6H. The PNCDFs are basically consistent at 1/6H and 5/6H, but they are different from the PNCDFs at the other three positions. This phenomenon is that due to the boundary effect, the cutting positions of 1/6H and 5/6H are close to the upper and lower boundaries. As the aggregate particles are not allowed to cross the model faces and edges, a different particle volume fraction and different morphology is expected close to the model boundaries. The cutting positions have negligible effect on 2D PNCDF of aggregate when they are not in the influence range of the boundary effect. Therefore, the cutting position is suggested to be close to 1/2H.

Moreover, four models with different sizes were developed, and they were model1 (250 × 250 × 50 mm), model2 (120 × 120 × 120 mm), model3 (100 × 100 × 100 mm), and model4 (80 × 80 × 80 mm). The PNCDF of each model was counted, and the time consumption for generating each model was recorded, as shown in Figure 5. It was found that the PNCDF of each model was basically the same and the time consumption for four models with descending order was model 1, model 2, model 3, and model 4, respectively. Thus, it can be concluded that 2D PNCDF of aggregate is independent of the model size and a model with small size should be selected to save time.

Finally, four models with different volume fractions of aggregate were generated, and they were model 1 (0.228), model 2 (0.295), model 3 (0.359), and model 4 (0.427). The PNCDF of each model is plotted in Figure 6. It is obvious

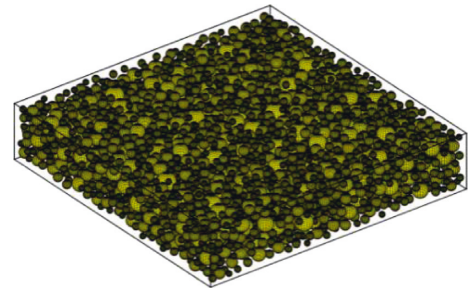

Figure 3: 3D random spherical aggregate model of L-RC2.

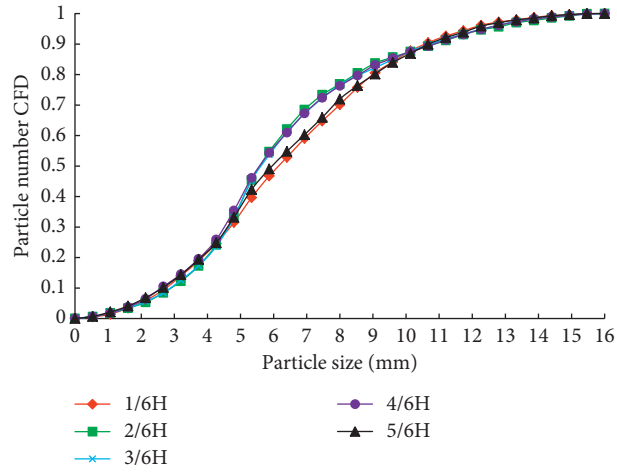

Figure 4: PNCDF at different cross-sectional positions.

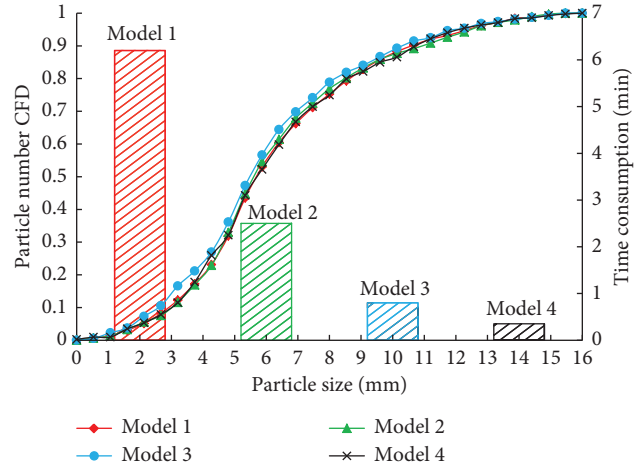

Figure 5: PNCDF and time consumption of different models.

that the PNCDF of each model is almost the same; thus, the volume fraction of aggregate is not considered as an influence factor on 2D PNCDF. From Figures 4–6, it also can be seen that the 2D PNCDF of coarse aggregate can be determined after the gradation curve of coarse aggregate is determined. For the L-RC2 specimen, the gradation curve of coarse aggregate with $\alpha = 0.5$ is described by equation (6).

2.1.3. 2D Random Polygonal Aggregate Model. In Zhang's experiment, the concrete specimen was 250 mm (length) × 250 mm (width) × 50 mm (height), natural river sand was used as fine aggregate. Ordinary Portland cement was used in the test. The volume fraction of coarse aggregates in L-RC2 is 0.395. According to the generating process of 2D random polygonal aggregate model shown in Figure 2, a 2D random polygonal aggregate model of cross section of L-RC2' 1/2H position is presented in Figure 7.

2.2. A Modified 2D Random Polygonal Aggregate Model Considering Porosity. Air bubbles produced during the mixing process have a significant effect on strength, shrinkage, and thermal conductivity of concrete. Based on the 2D random polygonal aggregate model, the "air bubbles" were employed to analyze the thermal conductivity of concrete more accurately. The porosity of concrete with no air-entraining agent was from 1% to 2% of concrete volume [26]. In this research, the porosity of concrete was 1.3%, and the diameter of each bubble was set to 2 mm. Finally, a modified 2D random polygonal aggregate model considering porosity is displayed in Figure 8.

2.3. Mesoscopic Numerical Model. After a 2D random polygonal aggregate model of concrete (geometrically) was generated, a mesoscopic numerical model was established by finite element method, and different material properties were directly assigned to the corresponding elements.

Developing a 2D random polygonal aggregate model of concrete along the thickness direction of L-RC2 is necessary when a mesoscopic numerical model was obtained to investigate the ETC of concrete. Actually, there always exist a laitance layer with 2~3 mm in thickness at the upper and lower surfaces of concrete, which causes the test data smaller than the actual ETC of concrete. To eliminate the influence of laitance on the ETC of concrete, a random polygonal aggregate model was conducted at 1/2H of L-RC2, and an alternative model with the same elevation dimensions as L-RC2 was cut, which is shown in Figure 9.

After a 2D random polygonal aggregate model of concrete (geometrically) was generated, a mesoscopic numerical model was established by using ANSYS, and different material properties were directly assigned to the corresponding elements. Finally, the mesoscopic numerical model of L-RC2 is presented in Figure 10.

2.4. Calculation Method of Effective Thermal Conductivity. In Fourier's law, the heat transfer rate Φ through a concrete slab is given in

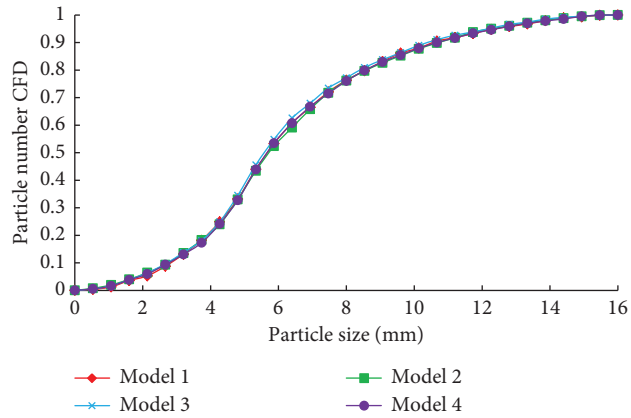

Figure 6: PNCDF with different volume fractions of aggregate.

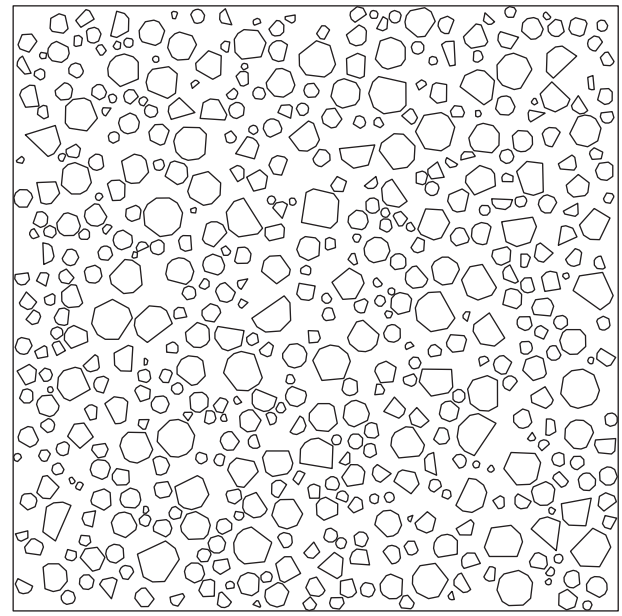

Figure 7: 2D random polygonal aggregate model of L-RC2 at the position of 1/2H.

$$\Phi = -\lambda A \frac{dT}{dx}, \tag{7}$$

where, λ is the thermal conductivity, A is the cross-sectional area, and T is temperature. And the heat flux q is derived from equation (7):

$$q = \frac{\Phi}{A} = -\lambda \frac{dT}{dx}. \tag{8}$$

Under the steady-state thermal conduction condition, the heat flux q within a concrete slab is calculated by

$$q = \frac{\Phi}{A} = \lambda \frac{\Delta T}{d}, \tag{9}$$

where ΔT is the temperature gradient and d is the thickness of specimen (in Figure 10).

The temperature gradient ΔT, the thickness d, and the area A are the controllable parameter in a mesoscopic

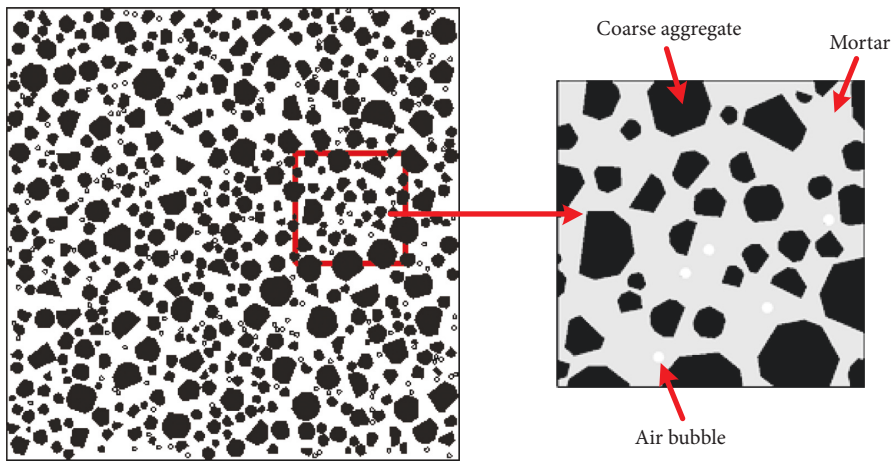

Figure 8: A modified model considering porosity.

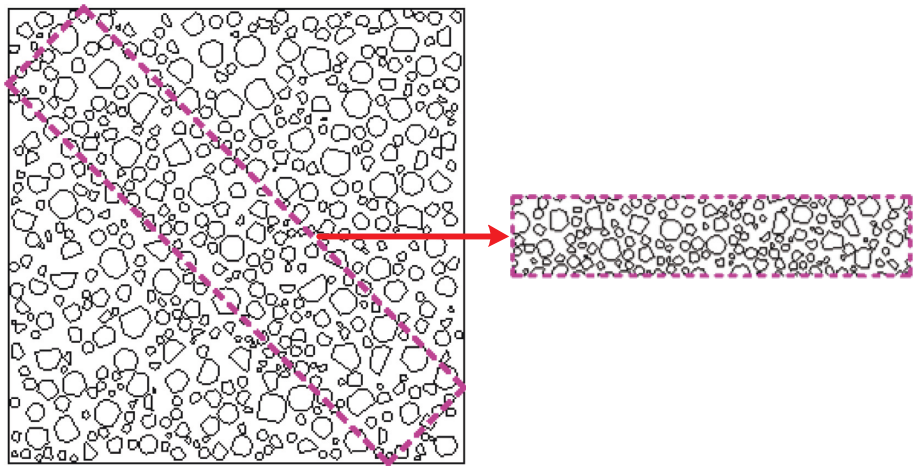

Figure 9: Cutting process of L-RC2 along the thickness direction.

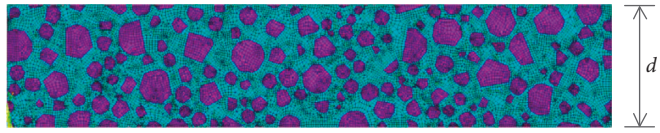

Figure 10: Mesoscopic model of L-RC2 (ANSYS).

numerical model, and the heat flux q can be calculated by equation (9). Then, the effective thermal conductivity λ_{ETC} can be written as equation (10) according to equation (9):

$$\lambda_{ETC} = \frac{q \cdot d}{\Delta T}. \tag{10}$$

3. Validation and Discussion

3.1. Parameters of the Test Model. To confirm the validity of mesoscopic numerical method for the ETC of concrete with arbitrary gradation, four specimens (L-RC1, L-RC5, L-RC6, and L-RC7) were selected from Zhang's experiment [10], and the mix proportions of four specimens are listed in Table 1 The other four specimens (basalt concrete, limestone concrete, siltstone concrete, and quartzite concrete) were from Khan's experiment [8]; then, the ETC of each specimen was calculated and compared with the experimental results.

In Khan's experiment, four different rocks (basalt, limestone, siltstone, and quartzite) were chosen as coarse aggregates for four concrete specimens with dimensions of 120 × 120 × 40 mm, and the natural river sand was used as fine aggregates. The volumetric mix proportions of all specimens were the same. Water: cement: fine aggregate: coarse aggregate was 0.203: 0.096: 0.261: 0.43 at a constant water-cement ratio of 0.60. The gradation curve used for the concrete specimens is given in Figure 11 and fitted by equation (1) with $\alpha = 2.5$.

Different thermal conductivity should be assigned to the corresponding elements calculating the ETC of concrete. In

Table 1: Mix proportions for selected specimens.

Specimen number	Water-cement ratio	Volume fraction				Volume fraction of aggregate
		Water	Cement	Fine aggregate	Coarse aggregate	
L-RC1	0.50	0.210	0.135	0.228	0.427	0.655
L-RC5	0.50	0.210	0.135	0.295	0.360	0.655
L-RC6	0.50	0.210	0.135	0.360	0.295	0.655
L-RC7	0.50	0.210	0.135	0.427	0.228	0.655

Zhang's experiment, the thermal conductivity of coarse aggregate is 2.487 W/m·K based on the test results, and different thermal conductivities of mortar with different volume fractions of the fine aggregates are given in Figure 12. It can be seen from Figure 12 that the thermal conductivity of mortar was linearly dependent to the volume fraction of fine aggregate. Then a linear fitted curve was also shown in Figure 12, and the thermal conductivity of mortar with arbitrary volume fraction of fine aggregate can be obtained by the linear interpolation. In Khan's experiment, the thermal conductivities of four different rocks were 4.03 W/m·K, 3.15 W/m·K, 3.52 W/m·K, and 8.58 W/m·K, respectively, under the dry state and the thermal conductivity of mortar was 1.37 W/m·K.

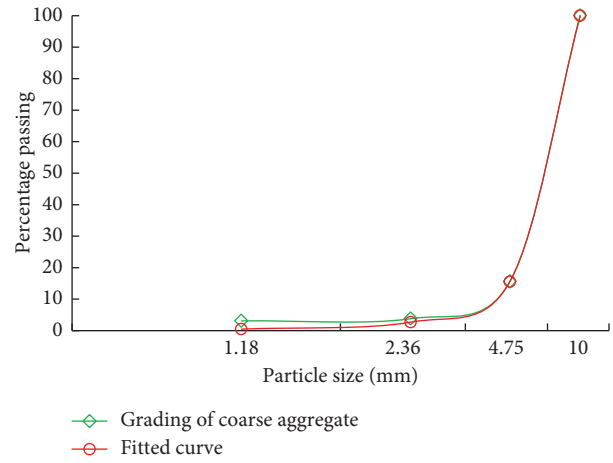

Figure 11: Gradation of coarse aggregate in Khan's experiment.

3.2. Results of the Mesoscopic Numerical Model without considering Porosity. According to the relevant parameters of test models from Zhang's and Khan's experiment, the 2D mesoscopic numerical models corresponding to the selected specimen are established and calculated, and the calculation results of heat flux are shown in Figures 13 and 14. It is evident from Figures 13 and 14 that the heat flux q of coarse aggregate is higher than that of cement mortar. This phenomenon confirms that the temperature in the aggregates transfers faster than that in the mortar. Another important conclusion is that the mesoscopic numerical model of concrete can reflect the influence of heterogeneity on concrete temperature field.

The thermal conductivity of selected specimens can be calculated by equation (10). In this equation, ΔT is set to 20K, d is determined by the specimen size, and the mean value of heat flux at the upper and lower surfaces is taken as the heat flux q in equation (10). The comparison between numerical results and experimental results for the thermal conductivity is shown in Figure 15. It is obvious that the thermal conductivities obtained by the mesoscopic numerical method are consistent with the test data from Zhang's experiment. Their relative deviation of thermal conductivity between numerical results and experimental values is from −3.04% to 6.62%, and the absolute deviation is from −0.053 to 0.102 W/m·K. However, for the thermal conductivity of four specimens in Khan's experiment, the numerical results are deviated from experimental values by 7.25% to 22.46%, and the absolute deviation is from 0.138 to 0.484 W/m·K. For larger deviation between numerical results and experimental values, the main reason is that the numerical model did not consider porosity and interface thermal resistance between coarse aggregate and mortar. However, Khan calculated the thermal conductivity of four

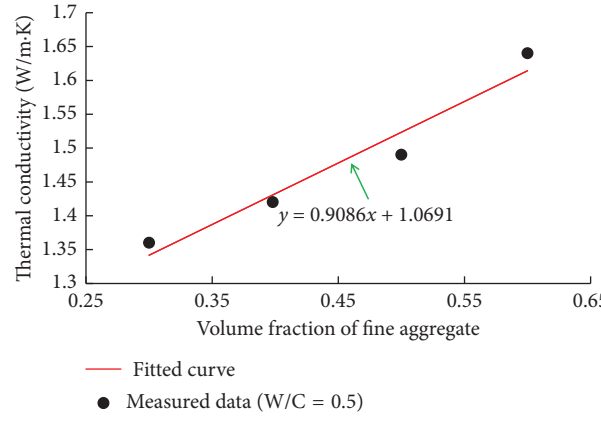

Figure 12: Thermal conductivity of mortar with different volume fractions of fine aggregate.

specimens by the Campbell–Allen and Thorne's model and Harmathy's model (as shown in Figures 15(b) and 16(b)), and their relative deviations were from 13% to 32% and 13.6% to 29.4%, respectively. The mesoscopic numerical method proposed in this paper significantly reduces the deviation from experimental values compared to the Campbell–Allen and Thorne's model and Harmathy's model.

3.3. Results of the Mesoscopic Numerical Model considering Porosity. The 2D mesoscopic numerical models corresponding to the selected specimens were also developed

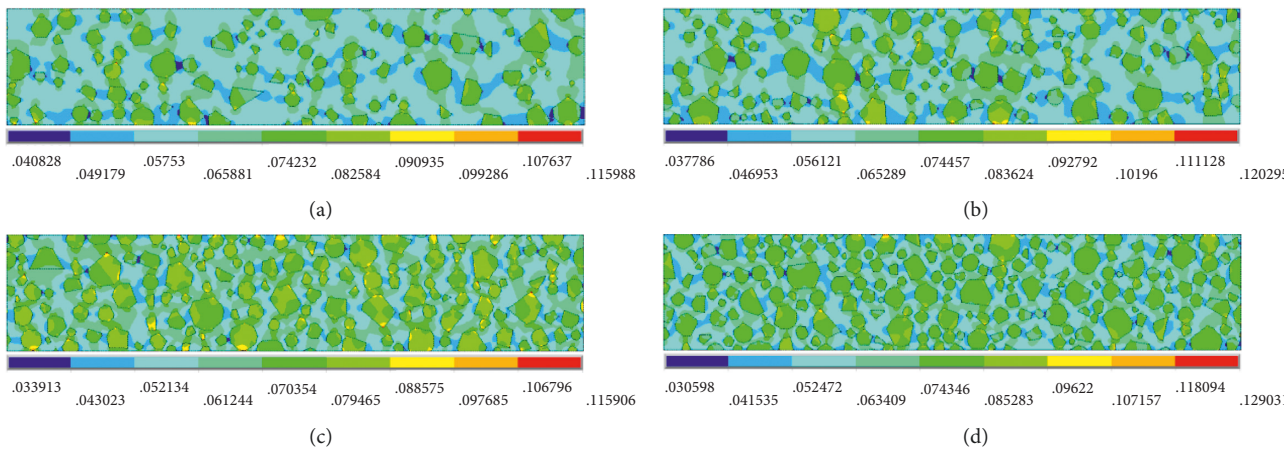

Figure 13: Numerical models from Zhang's experiment. (a) LR-1. (b) LR-5. (c) LR-6. (d)LR-7.

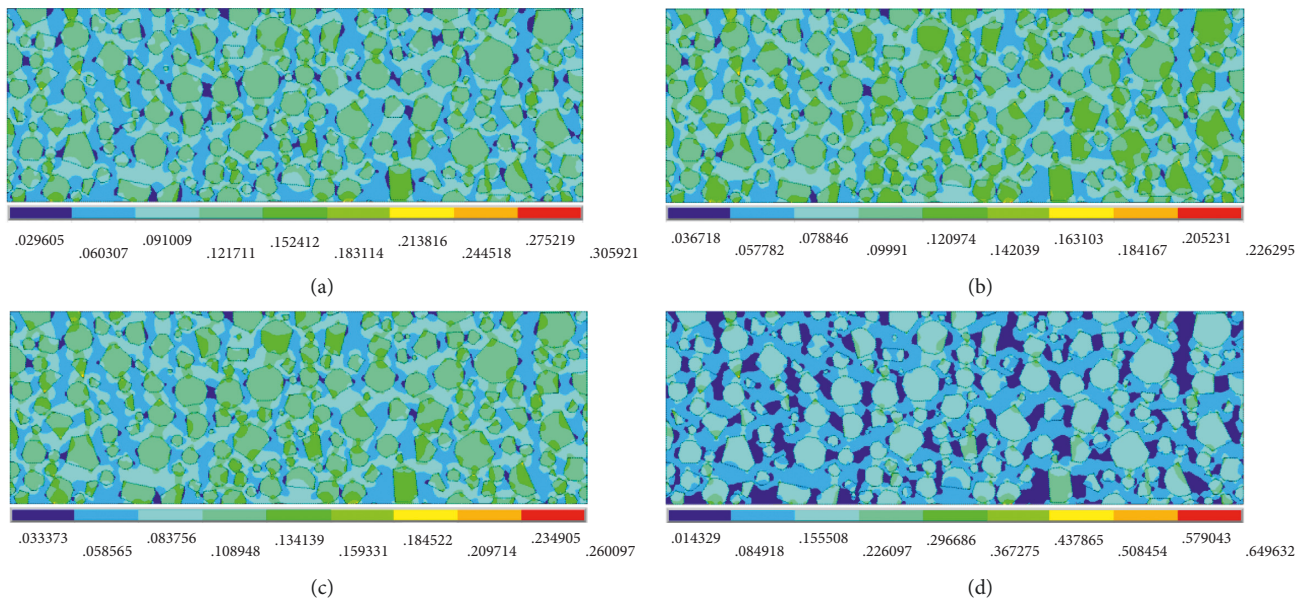

Figure 14: Numerical models from Khan's experiment. (a) Basalt concrete. (b) Limestone concrete. (c) Siltstone concrete. (d) Quartzite concrete.

considering the effect of porosity on the ETC of concrete, and the ETCs of four specimens were calculated. The comparison between the numerical results and experimental values for the thermal conductivity is shown in Figure 16. It can be found that the numerical results are closer to experimental values when the effect of porosity on thermal conductivity is considered. For the ETCs in Zhang's experiment, the relative deviation between the numerical results and experimental values is from −5.43% to 5.10%, and the absolute deviation is from −0.095 to 0.079 W/m·K. And for Khan's experiment, the relative deviation between the numerical results and experimental values is from 4.38% to 19.29%, and the absolute deviation is from 0.084 to 0.396 W/m·K. The mesoscopic numerical method considering porosity can predict a satisfactory ETC of concrete in terms of absolute deviation of thermal conductivity.

4. Parametric Analysis

It has been confirmed that the thermal conductivity of coarse aggregate and cement mortar as well as volume fraction of coarse aggregate has a significant effect on the ETC of concrete [7, 10, 27], but how these parameters affect the thermal conductivity of concrete is not clear. Therefore, a parametric analysis was conducted to clarify the effect of these parameters on the ETC of concrete based on the mesoscopic numerical method, and three different parameter conditions were set.

Parameter condition 1: the thermal conductivities of mortar and coarse aggregate were set to 1.396 W/m·K and 2.487 W/m·K, and the volume fraction of coarse aggregates was set to 0.228, 0.295, 0.36, 0.427, and 1, respectively.

Parameter condition 2: the thermal conductivity of mortar was set to 1.396 W/m·K, and the volume fraction of

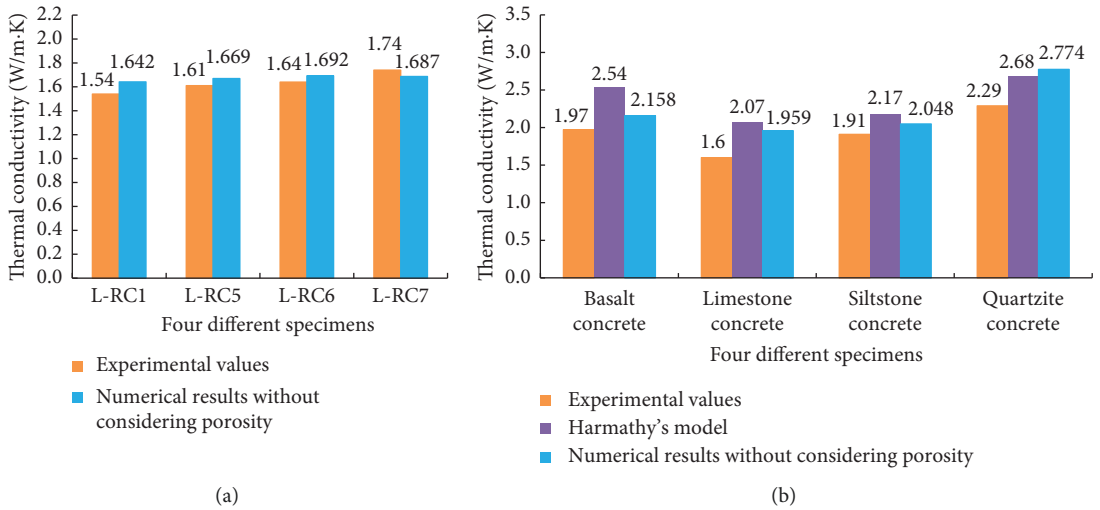

Figure 15: Comparison between numerical results and experimental values (without considering porosity). (a) Zhang's experiment. (b) Khan's experiment.

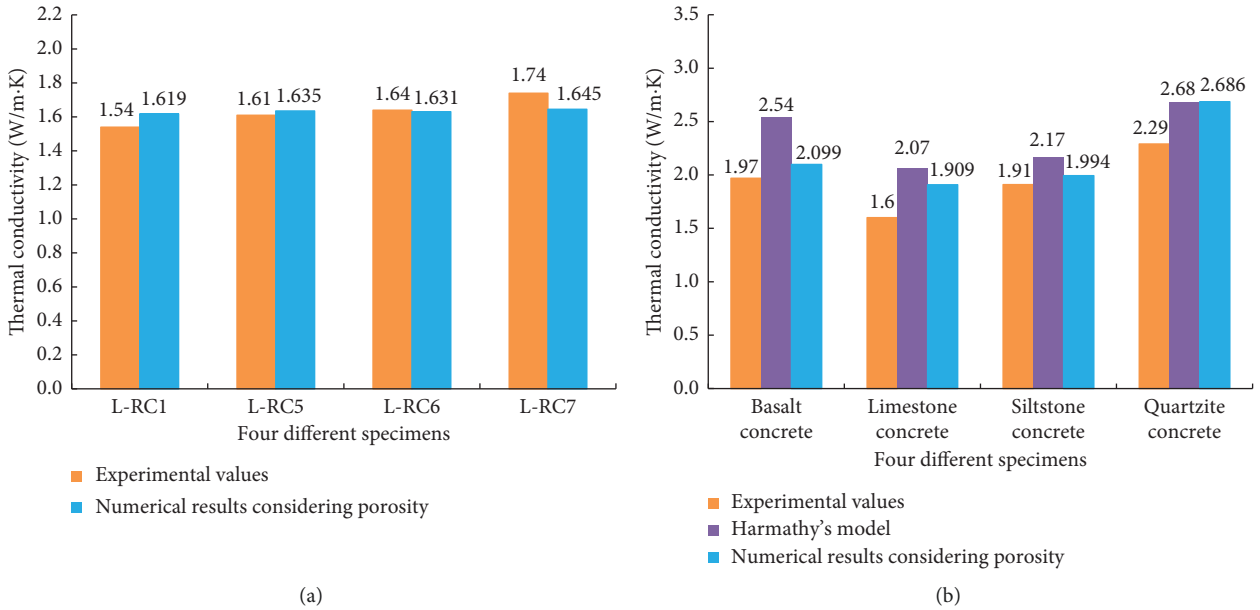

Figure 16: Comparison between numerical results and experimental values (considering porosity). (a) Zhang's experiment. (b) Khan's experiment.

coarse aggregate was set to 0.36. If the coarse aggregates were replaced by the magnetite, the maximum thermal conductivity of coarse aggregate (iron ore) was about 35 W/m·K. Thus, the thermal conductivities of coarse aggregates were set to 2.487 W/m·K, 4.03 W/m·K, 8.58 W/m·K, 15 W/m·K, 25 W/m·K, and 35 W/m·K, respectively.

Parameter condition 3: the thermal conductivity of coarse aggregate was set to 2.487 W/m·K, and the volume fraction of coarse aggregate was set to 0.36. In Liu's experiment [28], the iron ore sand was used as the fine aggregate to prepare the iron ore sand cement mortar, and the effective thermal conductivity of mortar was investigated at various replacement levels. The thermal conductivity of cement mortar reached 2.522 W/m·K when the fine aggregate was completely replaced by the iron ore sand. The thermal conductivities of mortar were set to 1.276 W/m·K, 1.694 W/m·K, 2.134 W/m·K, and 2.522 W/m·K, respectively, combined with Zhang's and Liu's experiment.

The ETCs of concrete with the dimension of 250 × 250 × 50 mm were calculated under three different parameter conditions. At the same time, the curve fitting of discrete points (numerical simulation results of ETC) was also performed, and the equations describing the corresponding fitting curves were also given, as shown in Figure 17. It is shown that a positive exponential correlation exists between the ETC of concrete and volume fraction of coarse

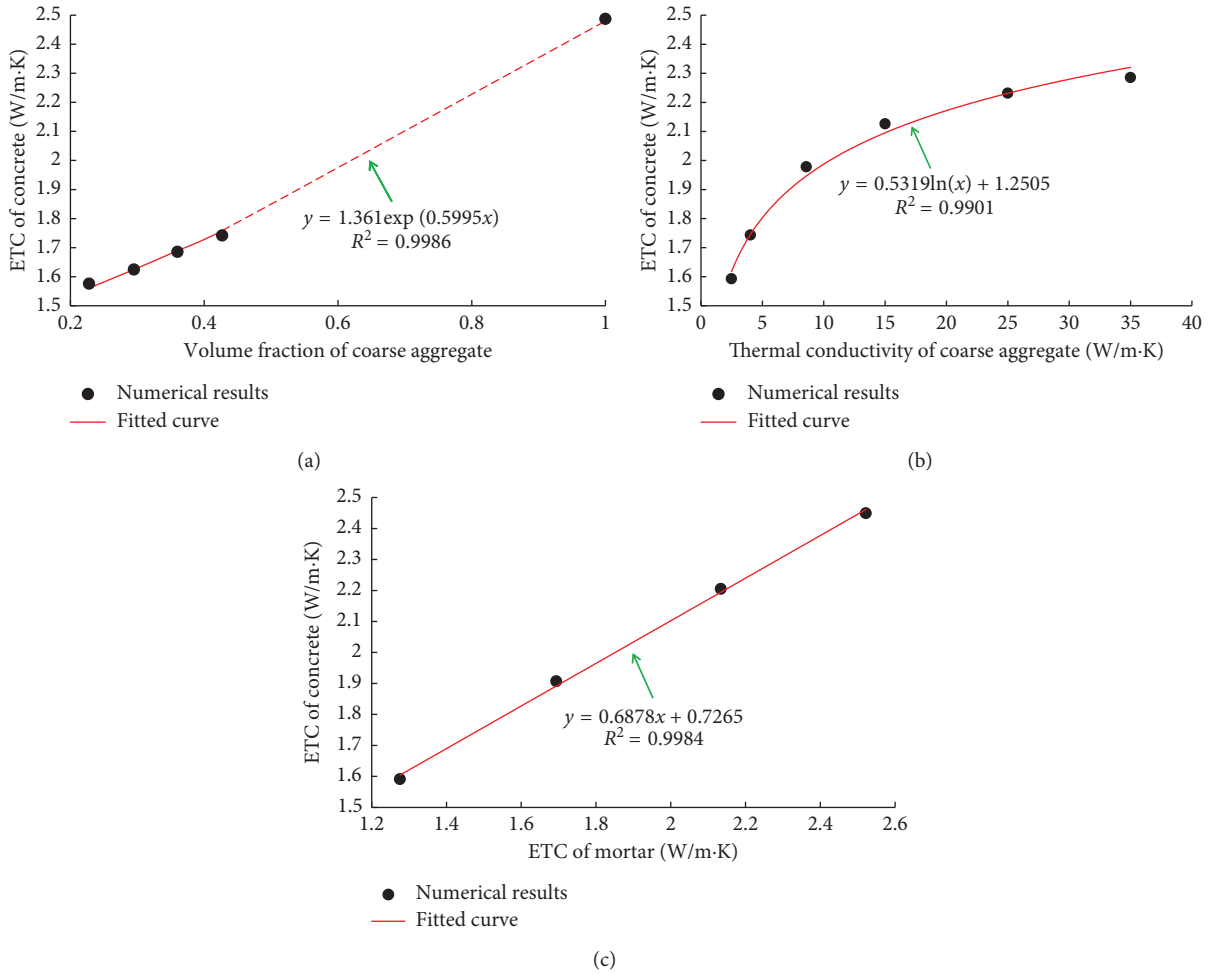

Figure 17: ETC of concrete specimens. Parameter condition: (a) 1, (b) 2, and (c) 3.

aggregates. Meanwhile, the ETC of concrete has a positive logarithm relationship with the thermal conductivity of coarse aggregate, and a positive linear correlation with the thermal conductivity of mortar. It can also be known from the Figure 17(a) that the change of aggregate volume fraction has a small influence on the ETC of concrete in the actual structure, and the variation range of ETC is less than 0.21 W/m·K.

Comparing Figures 17(b) and 17(c), it can be seen that the average growth rate of the ETC of concrete with the ETC of cement mortar is 0.69, which is 3.45 times faster than the maximum growth rate of the ETC of concrete with the thermal conductivity of coarse aggregates (0.2). This is because the coarse aggregates in the concrete are the discrete phase, but the heat transfer is mainly dependent on the continuous phase (cement mortar). From Figures 17(b) and 17(c), it can also be found that the ETC of concrete is 3.07 W/m·K when the coarse aggregates are completely replaced by the magnetite, but the ETC of concrete is less than 2.5 W/m·K when the ETC of cement mortar took the maximum within a reasonable range. In summary, the most practical way to improve the ETC of concrete is to increase the ETC of cement mortar, but the most effective way is to replace the coarse aggregate with an alternative material of a higher thermal conductivity.

5. Conclusions

This paper presents a mesoscopic numerical method to investigate the effective thermal conductivity of concrete with arbitrary gradation, and the influence factors of ETC of concrete were analyzed. The main conclusions are as follows:

(1) The mesoscopic numerical method for ETC of concrete with arbitrary gradation is proposed, and this method has been proved to be highly accurate.

(2) The two-dimensional gradation curve of coarse aggregate exists, and it is only related to the three-dimensional gradation curve of coarse aggregate.

(3) The generation method for a 2D random polygonal aggregate model of concrete with arbitrary gradation, and its modified model considering porosity are proposed.

(4) A positive exponential correlation exists between the ETC of concrete and volume fraction of coarse aggregates. Meanwhile, the ETC of concrete has a positive logarithm relationship with the thermal conductivity of coarse aggregate and a positive linear correlation with the thermal conductivity of mortar.

(5) In order to improve the ETC of concrete, the most practical way is to increase the ETC of cement mortar, but the most effective way is replacing the coarse aggregate with an alternative material of a higher thermal conductivity.

Data Availability

The data used to support the findings of this study are available from the corresponding author upon request.

Conflicts of Interest

The authors declare that they have no conflicts of interest.

Acknowledgments

This research was supported by the National Natural Science Foundation of China (grant nos. 51408484 and 51208056), Key R & D Projects in Shaanxi (grant no. 2018SF-359), and the Special Research Plan of Department of Education in Shaanxi (no. 14JK1488).

References

[1] X. Wang, Y. Zhang, W. Xiao, R. Zeng, Q. Zhang, and H. Di, "Review on thermal performance of phase change energy storage building envelope," *Science Bulletin*, vol. 54, no. 6, pp. 920–928, 2009.

[2] A. A. Adeyanju, T. O. Oni, and D. O. Akindele, "Experimental determination of thermophysical propertiesof concrete for thermal energy storage," *Journal of Engineering and Applied Sciences*, vol. 5, no. 4, pp. 282–289, 2010.

[3] L. Shen, Q. Ren, N. Xia, L. Sun, and X. Xia, "Mesoscopic numerical simulation of effective thermal conductivity of tensile cracked concrete," *Construction and Building Materials*, vol. 95, pp. 467–475, 2015.

[4] J. Lee, Y. Xi, and K. Willam, "Properties of concrete after high-temperature heating and cooling," *ACI Materials Journal*, vol. 105, no. 4, pp. 334–341, 2008.

[5] A. L. Marshall, "The thermal properties of concrete," *Building Science*, vol. 7, no. 3, pp. 167–174, 1972.

[6] M. J. Lu, S. Yang, X. Z. Feng, and S. B. Zhao, "Experimental study on thermal conductivity of concrete for building reinforced concrete composite wall," *Applied Mechanics and Materials*, vol. 438-439, pp. 329–332, 2013.

[7] J. Z. Xiao, Z. W. Song, and F. Zhang, "An experimental study on thermal conductivity of concrete," *Journal of Building Materials*, vol. 13, no. 1, pp. 17–21, 2010.

[8] M. I. Khan, "Factors affecting the thermal properties of concrete and applicability of its prediction models," *Building and Environment*, vol. 37, no. 6, pp. 607–614, 2002.

[9] K.-H. Kim, S.-E. Jeon, J.-K. Kim, and S. Yang, "An experimental study on thermal conductivity of concrete," *Cement and Concrete Research*, vol. 33, no. 3, pp. 363–371, 2003.

[10] W. Zhang, H. Min, X. Gu, Y. Xi, and Y. Xing, "Mesoscale model for thermal conductivity of concrete," *Construction and Building Materials*, vol. 98, no. 4, pp. 8–16, 2015.

[11] D. Campbell-Allen and C. P. Thorne, "The thermal conductivity of concrete," *Magazine of Concrete Research*, vol. 15, no. 43, pp. 39–48, 1963.

[12] T. Z. Harmathy, "Thermal properties of concrete at elevated temperatures," *Journal of Materials*, vol. 5, no. 1, pp. 47–74, 1970.

[13] R. L. Hamilton and O. K. Crosser, "Thermal conductivity of heterogeneous two-component systems," *Industrial and Engineering Chemistry Fundamentals*, vol. 1, no. 3, pp. 187–191, 1962.

[14] D. A. G. Bruggeman, "Berechnung verschiedener physikalischer Konstanten von heterogenen Substanzen. I. Dielektrizitätskonstanten und Leitfähigkeiten der Mischkörper aus isotropen Substanzen," *Annalen der Physik*, vol. 416, no. 7, pp. 636–664, 1935.

[15] D. P. H. Hasselman and L. F. Johnson, "Effective thermal conductivity of composites with interfacial thermal barrier resistance," *Journal of Composite Materials*, vol. 21, no. 6, pp. 508–515, 2016.

[16] X. Du, L. Jin, and G. Ma, "Numerical simulation of dynamic tensile-failure of concrete at meso-scale," *International Journal of Impact Engineering*, vol. 66, pp. 5–17, 2014.

[17] S.-M. Kim and R. K. Abu Al-Rub, "Meso-scale computational modeling of the plastic-damage response of cementitious composites," *Cement and Concrete Research*, vol. 41, no. 3, pp. 339–358, 2011.

[18] J. Xiao, W. Li, D. J. Corr, and S. P. Shah, "Effects of interfacial transition zones on the stress-strain behavior of modeled recycled aggregate concrete," *Cement and Concrete Research*, vol. 52, pp. 82–99, 2013.

[19] C. B. Du and L. G. Sun, "Numerical simulation of concrete aggregates with arbitrary shapes and its application," *Journal of Hydraulic Engineering*, vol. 37, no. 6, pp. 662–667, 2006.

[20] R. Ji, Z. Zhang, L. Liu, and X. Wang, "Development of the random simulation model for estimating the effective thermal conductivity of insulation materials," *Building and Environment*, vol. 80, pp. 221–227, 2014.

[21] S. Wei, C. Yiqiang, Z. Yunsheng, and M. R. Jones, "Characterization and simulation of microstructure and thermal properties of foamed concrete," *Construction and Building Materials*, vol. 47, no. 10, pp. 1278–1291, 2013.

[22] S. Tang, C. Tang, Z. Liang, Y. Zhang, and L. Li, "Numerical study of the influence of material structure on effective thermal conductivity of concrete," *Heat Transfer Engineering*, vol. 33, no. 8, pp. 732–747, 2012.

[23] J. K. Carson, S. J. Lovatt, D. J. Tanner, and A. C. Cleland, "An analysis of the influence of material structure on the effective thermal conductivity of theoretical porous materials using finite element simulations," *International Journal of Refrigeration*, vol. 26, no. 8, pp. 873–880, 2003.

[24] J. C. Walranen, "Theory and experiments on the mechanical behaviour of cracks in plain and reinforced concrete subjected to shear loading," *Civil Engineering and Geosciences*, vol. 26, 1981.

[25] X. Ruan and Z. C. Pan, "Mesoscopic simulation method of concrete carbonation process," *Structure and Infrastructure Engineering*, vol. 8, no. 2, pp. 1–12, 2011.

[26] W. Z. Wang and Z. X. Feng, "Influencing factors of fresh concrete air content," *Journal Chang'an University (National Science Education)*, vol. 29, no. 3, pp. 107–110, 2009.

[27] L. H. Zhu, J. Dai, G. L. Bai, and J. F. Zhang, "Experimental study on thermal conductivity of recycled concrete," *Journal of Building Materials*, vol. 18, no. 5, pp. 852–856, 2015.

[28] K. Liu, Z. Wang, C. Jin, F. Wang, and X. Lu, "An experimental study on thermal conductivity of iron ore sand cement mortar," *Construction and Building Materials*, vol. 101, pp. 932–941, 2015.